Supplement of

Quantifying key parameter sensitivities for water table depth in hydrological schemes of CoLM-PSUADE

Tingting Wu, Shupeng Zhang, Xiaofan Yang, and Yongjiu Dai

Correspondence to: Xiaofan Yang (xfyang@bnu.edu.cn)

S1: Results of qualitative sensitivity analysis

S1.1 Qualitative screening results

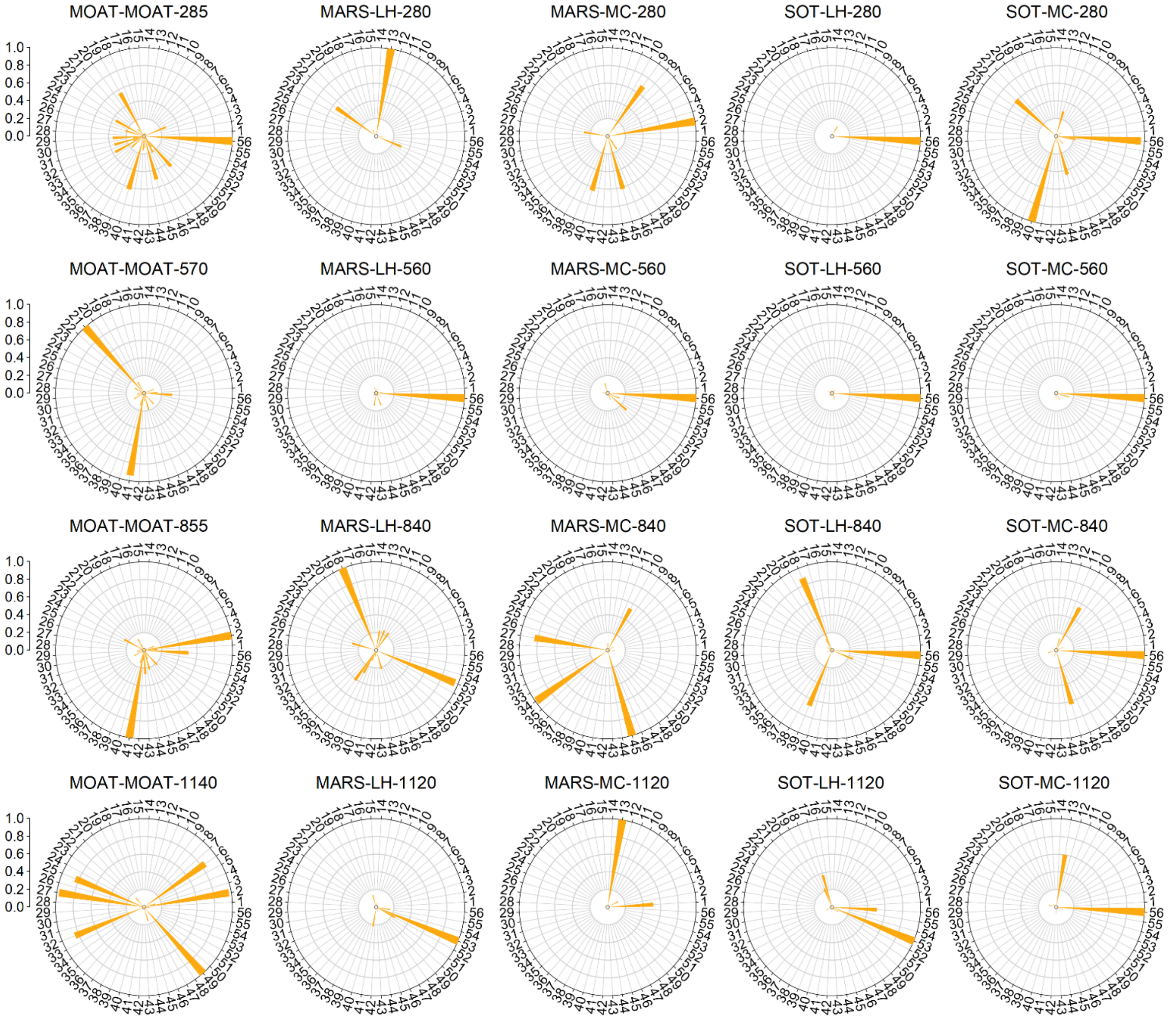

Figure S1: Qualitative sensitivity analysis results based on the *MAE* objective function. The numbers on the outer ring represent parameter indices (refer to Table 2 for the corresponding parameter definitions). The length of each pointer indicates the normalized sensitivity index, ranging from 0 to 1, with longer pointers denoting higher sensitivity. Each subplot title follows the format "sensitivity analysis method-sampling technique-sample size".

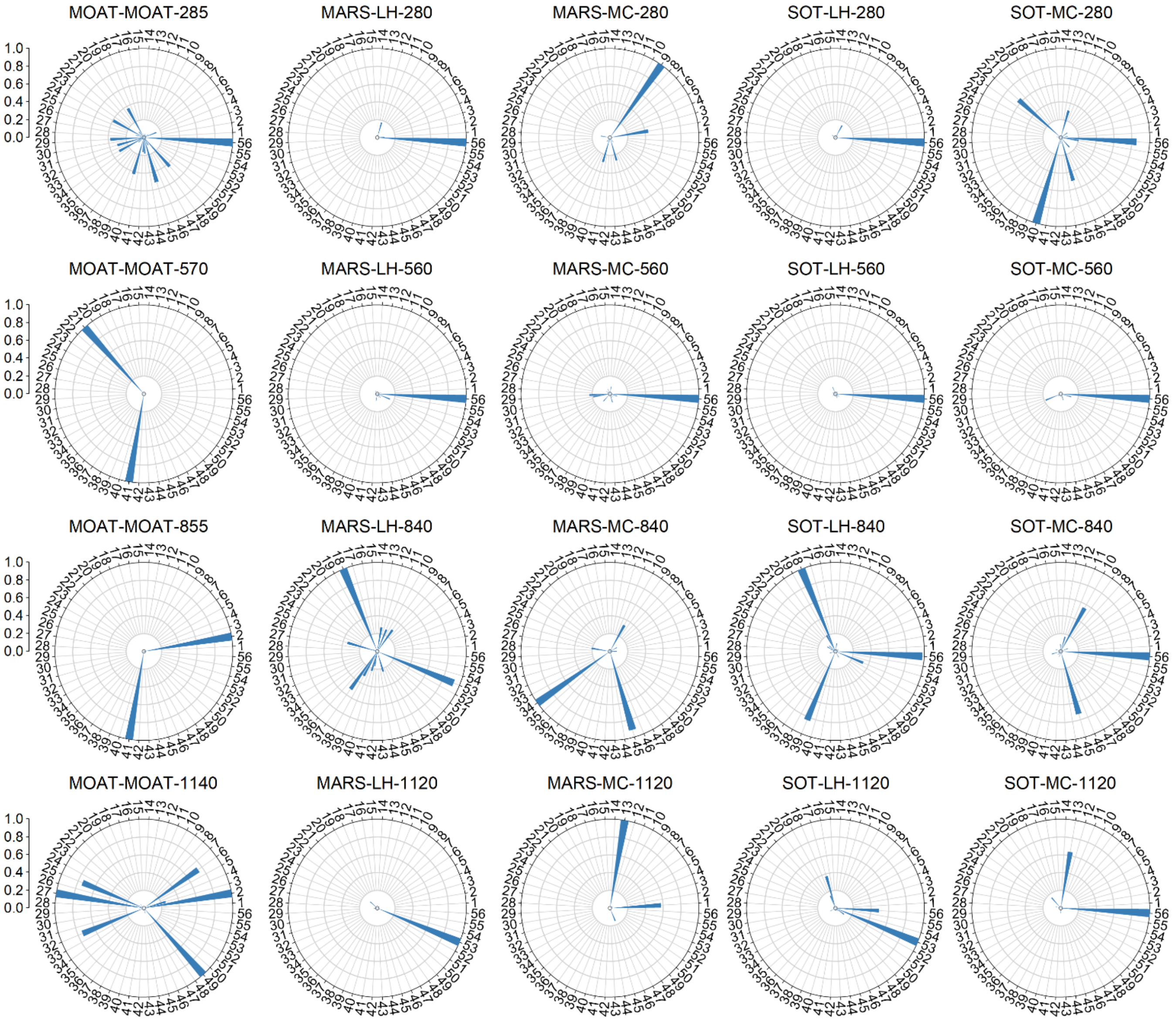

Figure S2: Qualitative sensitivity analysis results based on the R^2 objective function. The numbers on the outer ring represent parameter indices (refer to Table 2 for the corresponding parameter definitions). The length of each pointer indicates the normalized sensitivity index, ranging from 0 to 1, with longer pointers denoting higher sensitivity. Each subplot title follows the format "sensitivity analysis method-sampling technique-sample size".

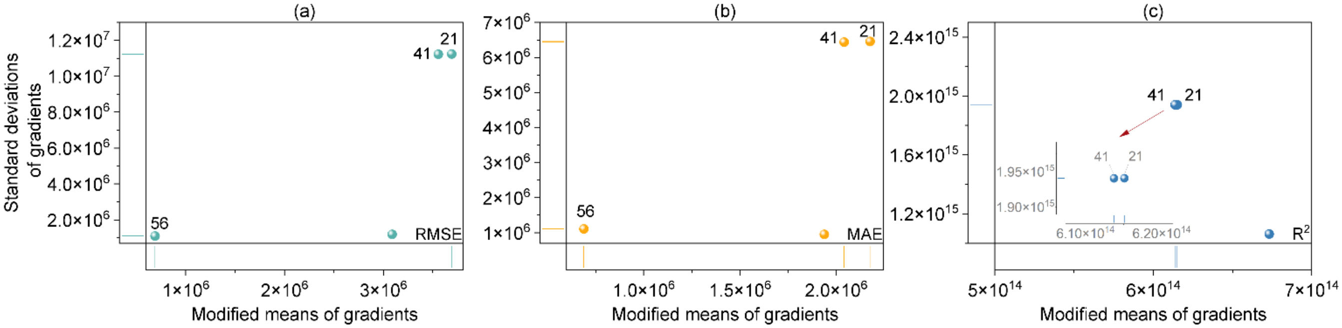

Figure S3. Sensitivity and interaction results from the MOAT method with a sample size of 570. The horizontal axis denotes the modified mean (μ_i^*), and the vertical axis denotes the standard deviation (σ_i^*). Subplots (a)–(c) correspond to the $RMSE$, MAE, and R^2 objective functions, respectively.

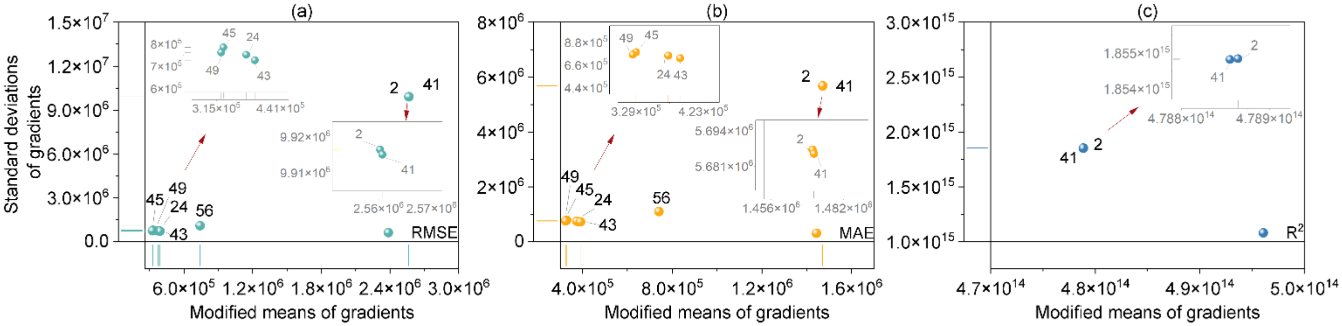

Figure S4. Sensitivity and interaction results from the MOAT method with a sample size of 855. The horizontal axis denotes the modified mean (μ_i^*), and the vertical axis denotes the standard deviation (σ_i^*). Subplots (a)–(c) correspond to the $RMSE$, MAE, and R^2 objective functions, respectively.

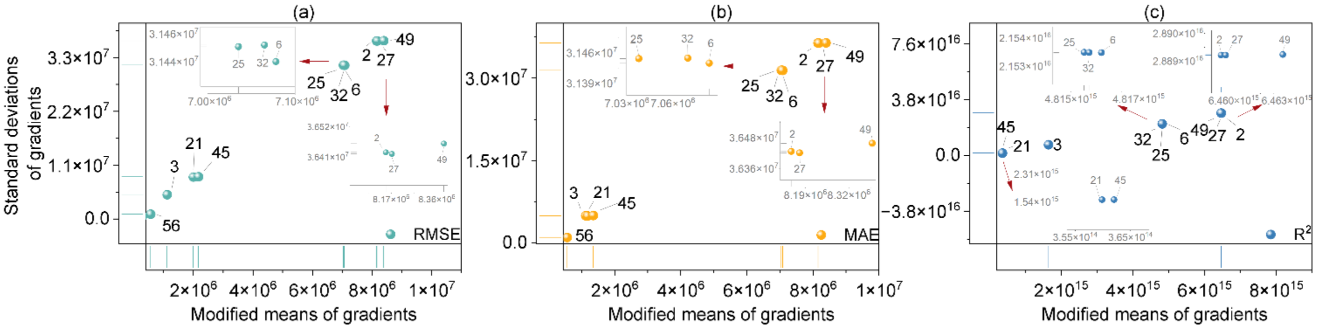

Figure S5. Sensitivity and interaction results from the MOAT method with a sample size of 1140. The horizontal axis denotes the modified mean (μ_i^*), and the vertical axis denotes the standard deviation (σ_i^*). Subplots (a)–(c) correspond to the $RMSE$, MAE, and R^2 objective functions, respectively.

S1.2 Sample quality check

To quantify the space-fillingness of a sample, PSUADE provides the command named ‘sqc’, which computes a few metrics such as the minimum distance between all pairs of sample points (the larger the better), the average minimum distance for all sample points (the larger the better) and the minimum distance between the sample points and the corners (the smaller the better). However, the average minimum distances between all points and corners are not calculated when the number of input parameters is greater than 30. For the qualitative sensitivity experiment, since the input dimension is 56, only the first two distance indicators were calculated based on the normalized sampling results (Table S1).

Table S1: Sample quality check for qualitative sensitivity analysis.

Method	Sampling technique	Avg-min distance	Min-min distance
MARS-5times	MC	3.041	2.063
MARS-10times		3.043	1.890
MARS-15times		3.043	1.954
MARS-20times		3.040	1.844
SOT-5times	LH	3.051	2.051
SOT-10times		3.048	1.981
SOT-15times		3.047	2.011
SOT-20times		3.047	1.936
MOAT-5times	MOAT	3.932	0.667
MOAT-10times		4.005	0.667
MOAT-15times		4.073	0.667
MOAT-20times		4.062	0.667

The sampling quality metrics exhibit clear differences among the three sampling strategies. For the MARS and SOT methods, the average minimum distance (Avg-min distance) remains nearly constant at approximately 3.04–3.05 as the sample size increases, indicating that both approaches maintain a stable level of global space-filling capability. In contrast, their minimum pairwise distance (Min-min distance) shows a slight decreasing trend with increasing sample size, reflecting the expected densification of sample points in high-dimensional space as more samples are added. In contrast, the Avg-min distance for MOAT is significantly larger (ranging from 3.93 to 4.07) than those of MARS and SOT, indicating that sample points are more widely separated on average. Meanwhile, its Min-min distance remains constant at 0.667 regardless of sample size, reflecting the deterministic and grid-based nature of its trajectory design. This behaviour underscores that MOAT prioritizes structured one-at-a-time perturbations rather than achieving uniform coverage of the multidimensional input space.

Overall, the results demonstrate that MARS and SOT achieve a better balance between global coverage and local separation, making them more suitable for space-filling experimental design, while MOAT is inherently limited by its trajectory-based structure.

S2: Results of quantitative validation of key sensitivity parameters

According to the response surface validation results across different experiments (Table S2), the error metrics Err_{rmss} and Err_{maxs} showed relatively high values. However, they were still 1–2 orders of magnitude smaller than the overall variation range of the sample outputs (Table S3). Further evaluation using Err_{maxs2} was therefore necessary. After min-max normalization, all Err_{maxs2} values were less than 1, and most of the average errors Err_{avgs} did not deviate significantly from 1, indicating that the accuracy of the response surfaces was acceptable. Furthermore, the coefficient of determination R^2_{rsm} from cross-validation was above 0 (0.122–0.658) when a GP was used as the response surface model. After applying a logarithmic transformation to the outputs (logGP), R^2_{rsm} increased to above 0.7 (0.726–0.837). For the parameter sets with input dimensions of 12 and 21, the remaining errors decreased by orders of magnitude. These results indicated that the response surfaces trained on the loaded samples (constructed from input parameters and $RMSE$ outputs) were of good quality, and also suggested that the output range influenced the fitting accuracy. In addition, the data points in the corresponding diagnostic plots were closely distributed along the diagonal (Fig. S6–Fig. S8), further supporting this conclusion. Based on the above evaluation metrics, both GP and logGP response surfaces can be considered reliable and suitable for subsequent quantitative sensitivity analysis.

Table S2: Response surface cross-validation metrics.

Experiment[a]	Response surface	Err_{avgs}	Err_{rmss}	Err_{maxs}	Err_{maxsb}	Err_{maxs2}	R^2_{rsm}
8-50times	GP	1.623	16.820	174.700	0.610	0.711	0.372
	logGP	1.669	29.360	633.700	0.005	0.687	0.786
8-100times	GP	6.079	64.540	1531.000	0.478	0.678	0.203
	logGP	11.310	236.400	7401.000	6.712×10^{-5}	0.687	0.726
8-150times	GP	5.542	73.020	937.600	1.302	0.900	-
	logGP	10.950	304.400	1.173×10^{4}	6.712×10^{-5}	0.625	0.792
12-40times	GP	1. 284	41.610	435.800	1.100	0.902	0.122
	logGP	0.449	5.700	78.810	0.036	0.734	0.737
12-80times	GP	1.713	37.850	568.900	1.100	0.705	0.548
	logGP	0.412	6.750	103.700	0.040	0.748	0.758
12-100times	GP	1.466	44.420	616.900	0.659	0.483	0.804

	logGP	0.539	7.261	159.900	0.017	0.620	0.818
21-20times	GP	299.200	4966.000	1.043×10^{5}	0.637	0.894	0.658
	logGP	1.382	9.868	118.800	0.008	0.670	0.832
21-40times	GP	2.655×10^{4}	4.782×10^{5}	7.188×10^{6}	0.365	1.000	-
	logGP	0.618	7.354	129.800	0.008	0.962	0.746
21-100times	GP	1.672×10^{4}	3.869×10^{6}	9.006×10^{7}	0.514	1.201	-
	logGP	2.328	53.590	2166.000	7.869×10^{-5}	0.921	0.837

[a]“$\boldsymbol{n}$-$\boldsymbol{k}$ times” in the column of “Experiment” denotes an experimental configuration with $\boldsymbol{n}$ input parameters and a sample size equal to $\boldsymbol{k}$ times the number of parameters. In the software implementation, the actual number of model runs (sample sizes) is $\boldsymbol{k} \times (\boldsymbol{n} + \boldsymbol{2})$.

Table S3: Range of RMSE outputs in the RSMSobol analysis experiments.

Experiment[a]	Response surface	Sample Output$_{\text{min}}$	Sample Output$_{\text{max}}$
8-50 times	GP	4.783662×10^{-1}	1.192372×10^{3}
	logGP	-7.373787×10^{-1}	7.083700
8-100 times	GP	4.783662×10^{-1}	1.467529×10^{3}
	logGP	-7.373787×10^{-1}	7.291335
12-40 times	GP	3.924328×10^{-1}	1.625459×10^{3}
	logGP	-9.353899×10^{-1}	7.393545
12-80 times	GP	3.827627×10^{-1}	2.079594×10^{3}
	logGP	-9.603402×10^{-1}	7.639928
12-100 times	GP	3.827627×10^{-1}	3.835408×10^{3}
	logGP	-9.603402×10^{-1}	8.252031
21-20 times	GP	3.812231×10^{-1}	1.847612×10^{5}
	logGP	-9.643704×10^{-1}	1.212682×10^{1}
21-40 times	GP	3.190905×10^{-1}	3.820296×10^{7}
	logGP	-1.142281	1.745842×10^{1}
21-100 times	GP	3.190905×10^{-1}	3.856754×10^{7}
	logGP	-1.142281	1.746792×10^{1}

[a]“$\boldsymbol{n}$-$\boldsymbol{k}$ times” in the column of “Experiment” denotes an experimental configuration with $\boldsymbol{n}$ input parameters and a sample size equal to $\boldsymbol{k}$ times the number of parameters. In the software implementation, the actual number of model runs (sample sizes) is $\boldsymbol{k} \times (\boldsymbol{n} + \boldsymbol{2})$.

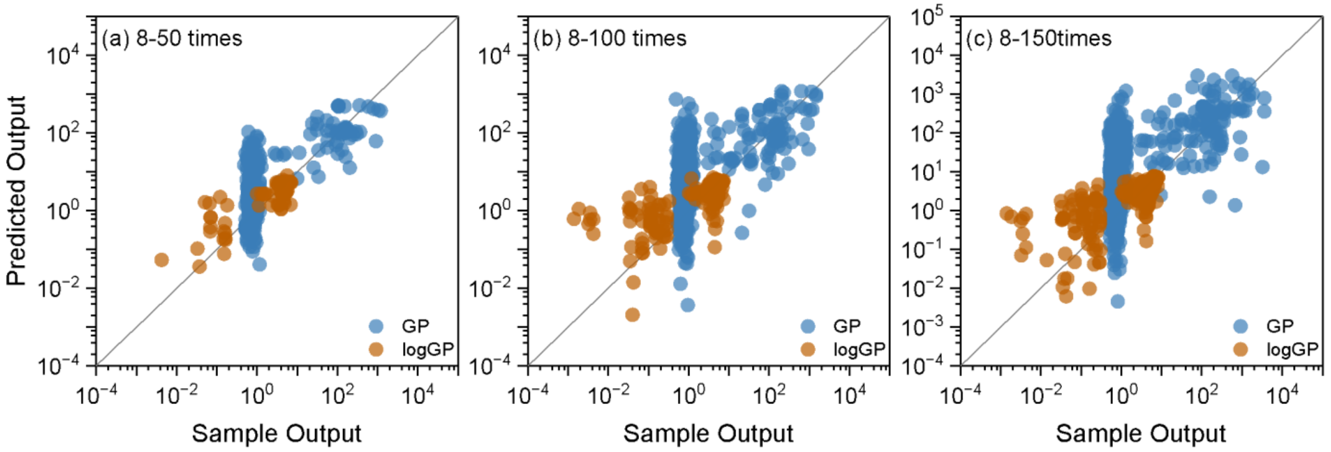

Figure S6: Response surface cross-validation scatter plot for the case where the input dimension is 8.

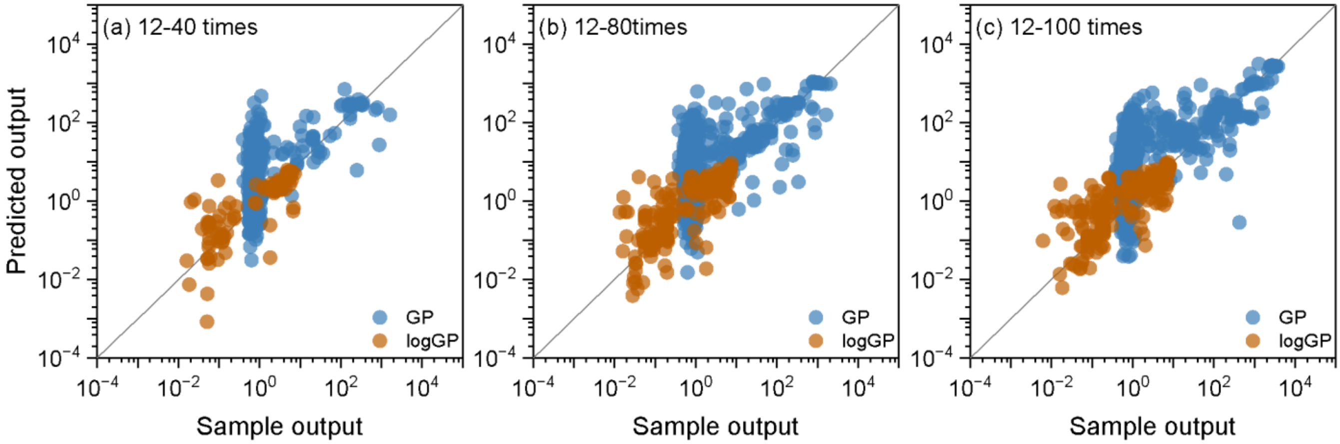

Figure S7: Response surface cross-validation scatter plot for the case where the input dimension is 12.

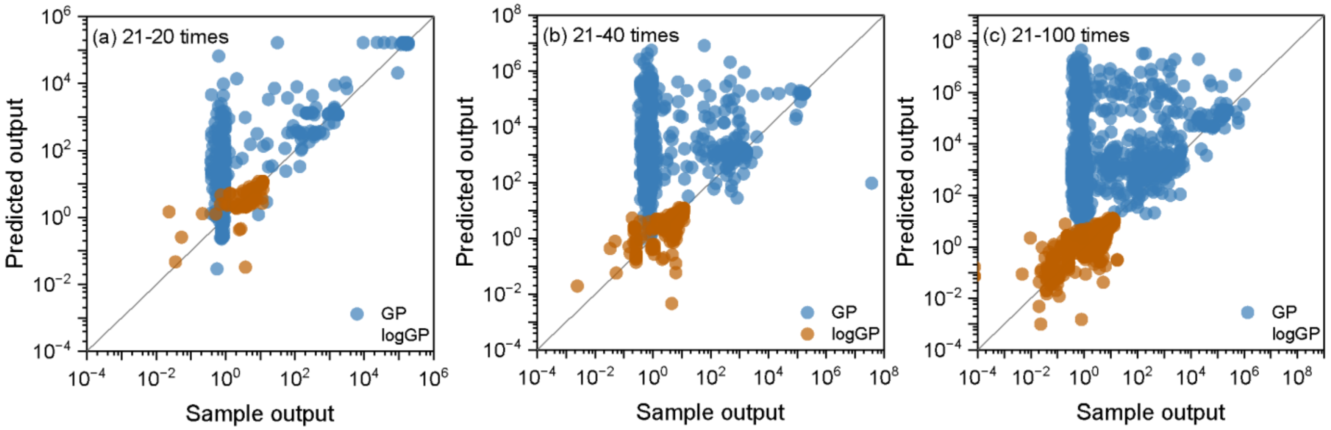

Figure S8: Response surface cross-validation scatter plot for the case where the input dimension is 21.

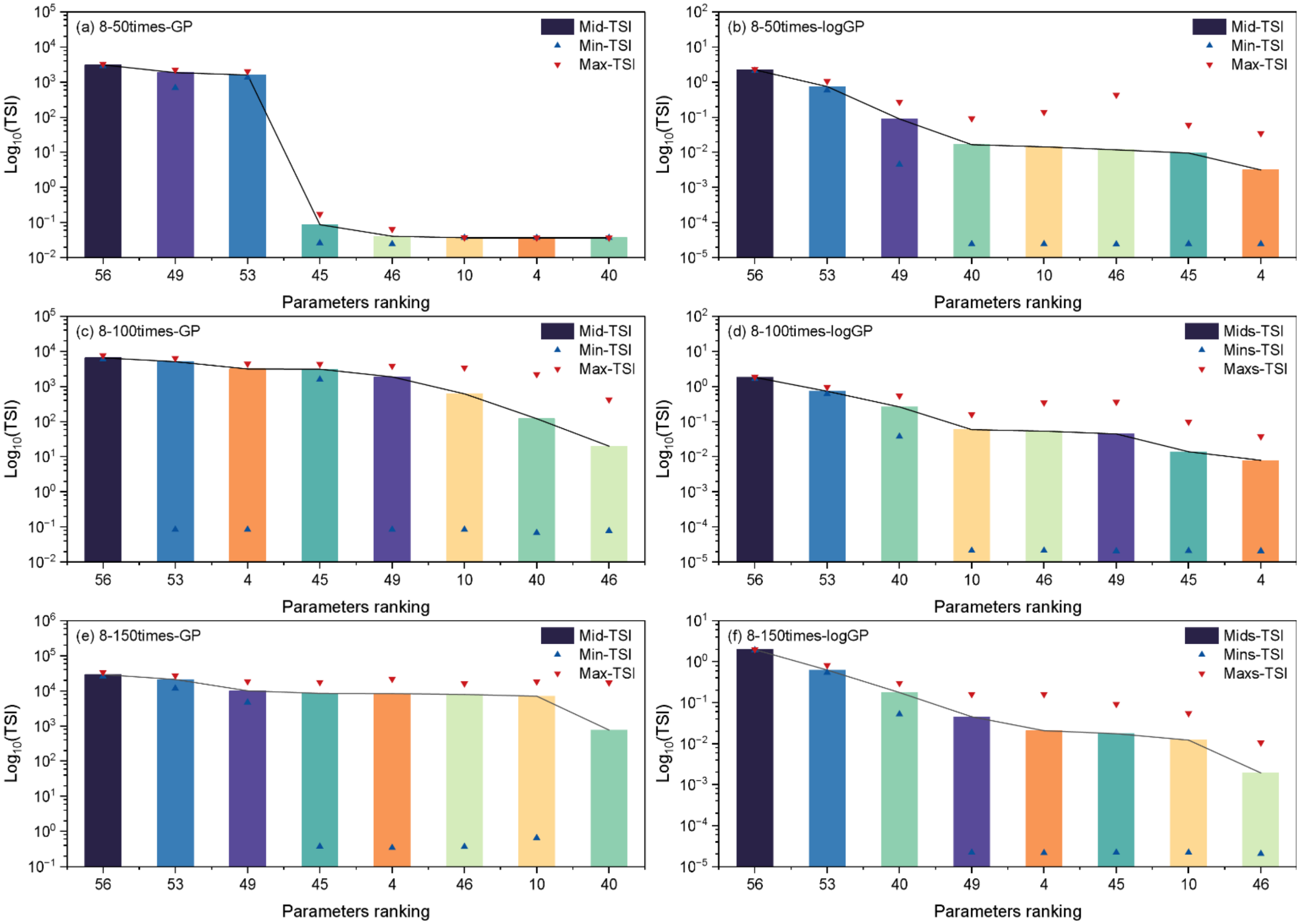

Figure S9: The ranking results of quantitative sensitivity indicators when the input dimension is 8.

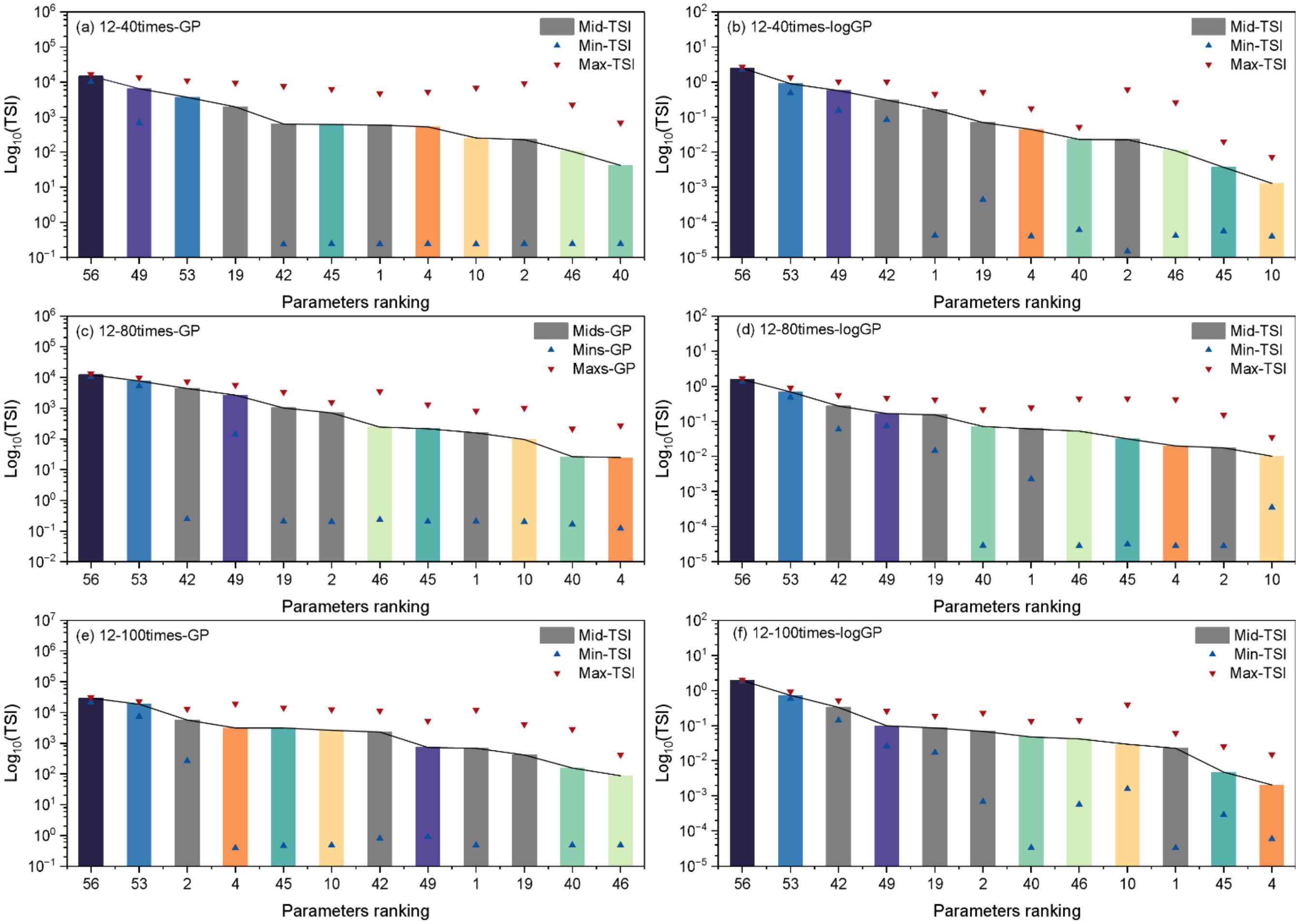

Figure S10: The ranking results of quantitative sensitivity indicators when the input dimension is 12.

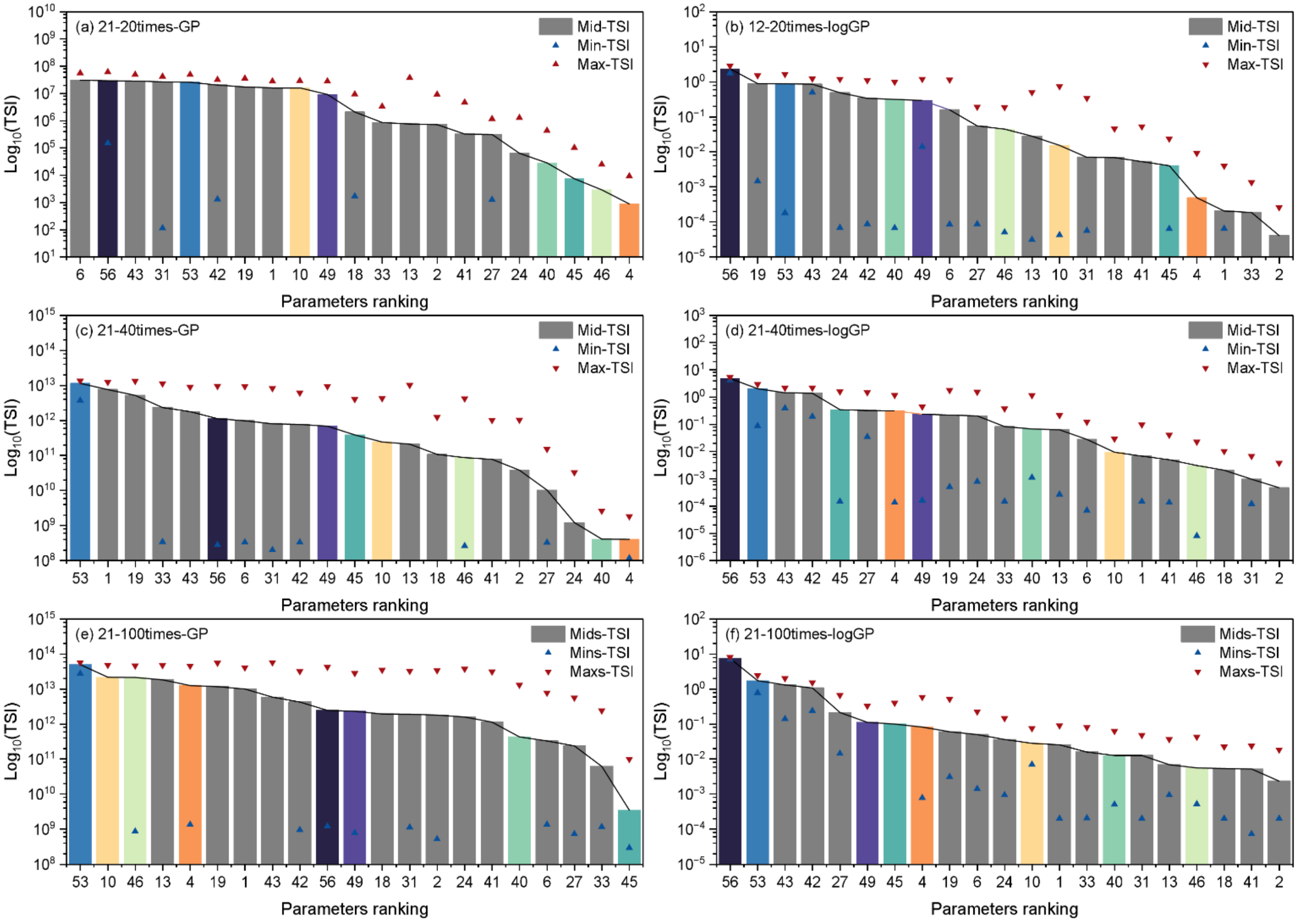

Figure S11: The ranking results of quantitative sensitivity indicators when the input dimension is 21.

S3: Results of optimal estimation of key sensitivity parameters

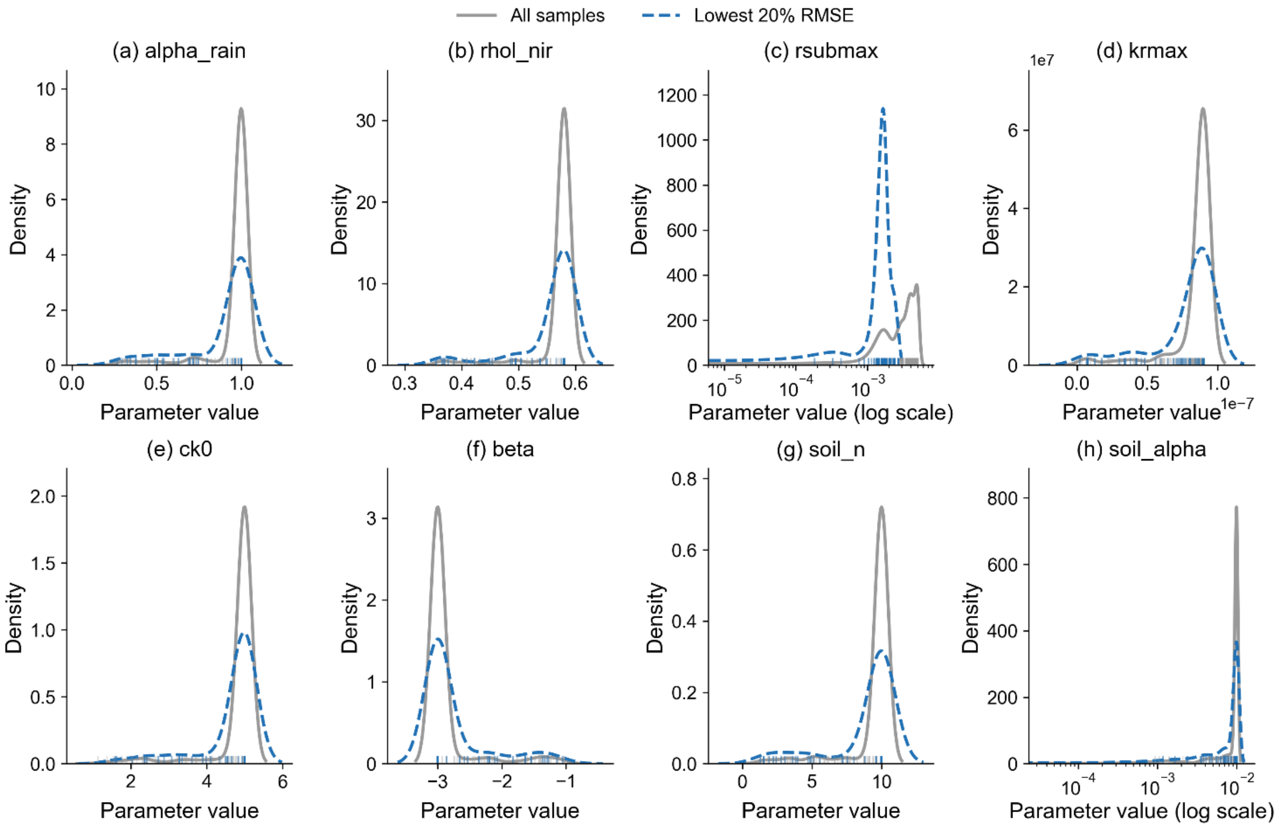

Figure S12: Comparison of KDE for the top 20% low-$RMSE$ parameter sets (blue) versus the entire set of 500 evaluations (grey) obtained by the PSO method: (a) alpha_rain, (b) rhol_nir, (c) rsubmax, (d) krmax, (e) ck0, (f) beta, (g) soil_n, and (h) soil_alpha.

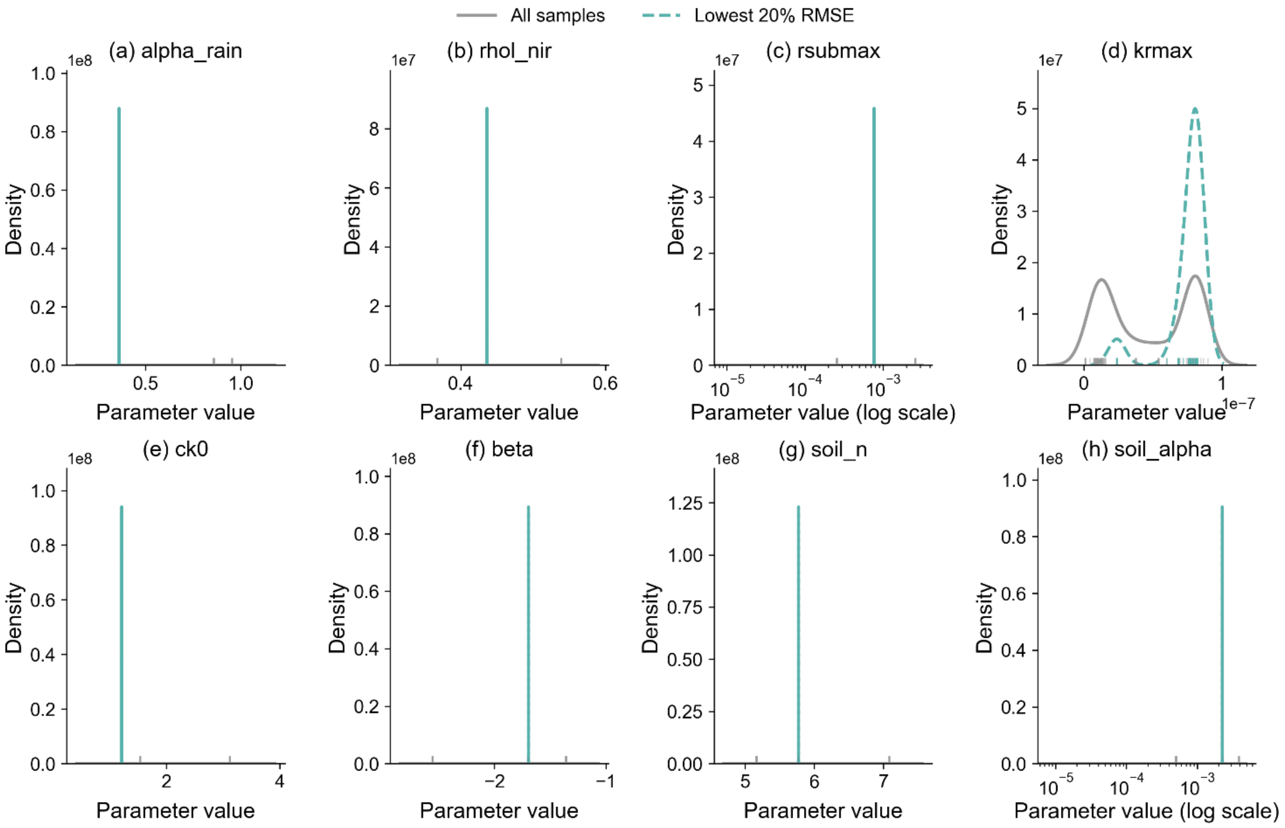

Figure S13: Comparison of KDE for the top 20% low-$RMSE$ parameter sets (green) versus the entire set of 500 evaluations (grey) obtained by the BOBYQA method: (a) alpha_rain, (b) rhol_nir, (c) rsubmax, (d) krmax, (e) ck0, (f) beta, (g) soil_n, and (h) soil_alpha.

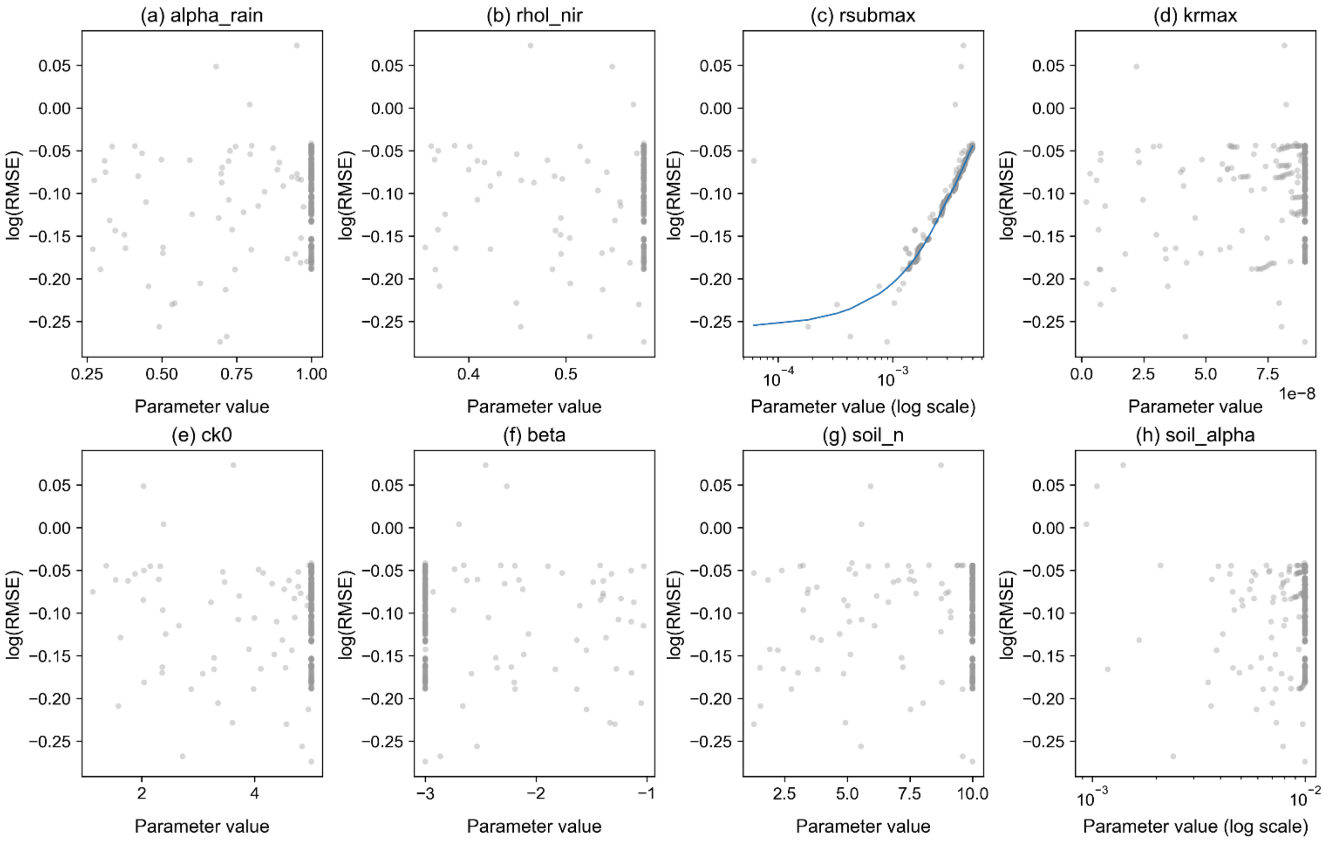

95 **Figure S14: Scatter plots of $RMSE$ against parameter values based on 500 evaluations obtained during the PSO optimization process: (a) alpha_rain, (b) rhol_nir, (c) rsubmax, (d) krmax, (e) ck0, (f) beta, (g) soil_n, and (h) soil_alpha.**

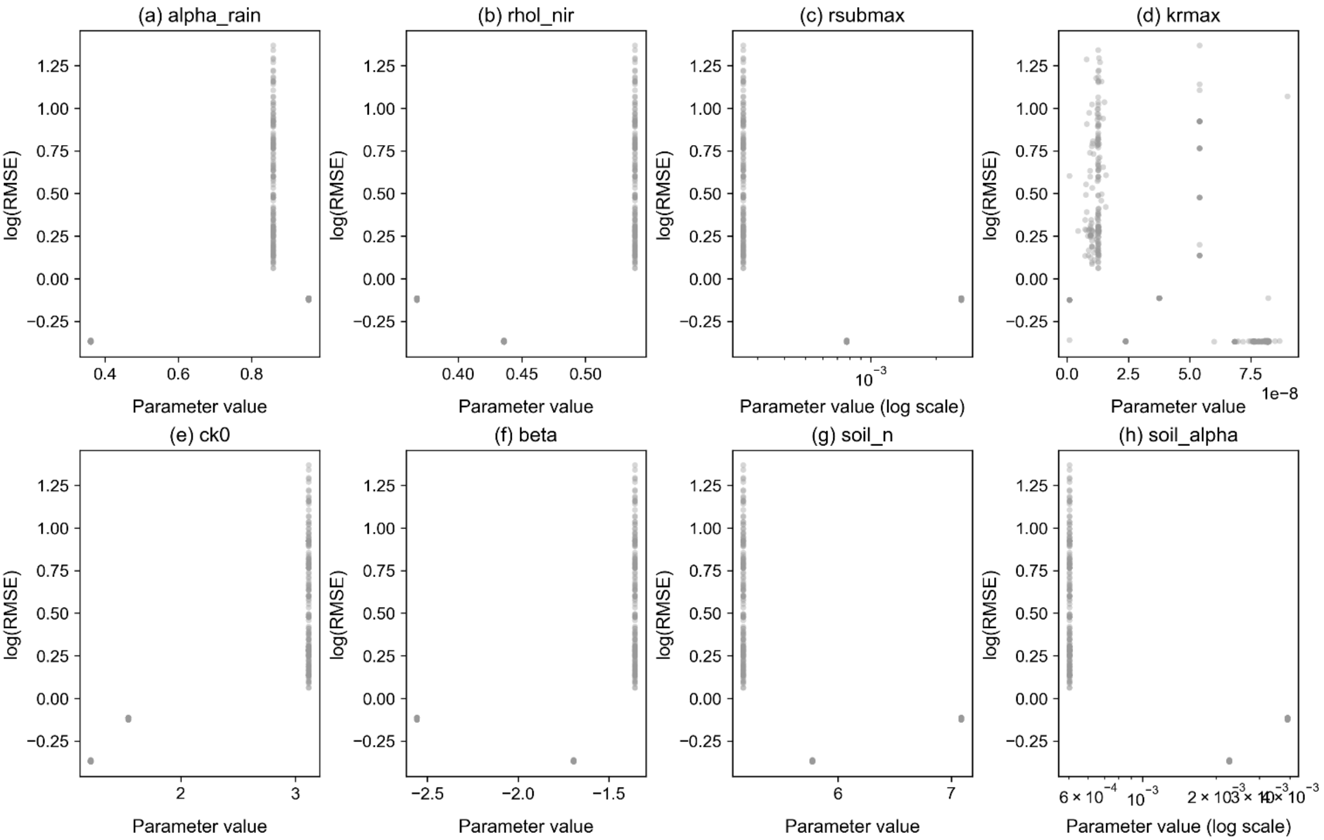

Figure S15: Scatter plots of $RMSE$ against parameter values based on 500 evaluations obtained during the BOBYQA optimization process: (a) alpha_rain, (b) rhol_nir, (c) rsubmax, (d) krmax, (e) ck0, (f) beta, (g) soil_n, and (h) soil_alpha.

S4: Mathematical formulations of eight stably sensitive parameters

This section provides the detailed governing equations for the parameters identified as stably sensitive to water table depth (WTD) dynamics in CoLM. Table S4 lists these parameters.

Table S4: Summary of the eight sensitive parameters.

Variable Name	Parameter Symbol	Reference Section
56-soil_alpha	α	Sect S4.1
53-soil_n	n	Sect S4.1
40-rsubmax	$r_{sub,max}$	Sect S4.2
49-beta	β	Sect S4.3

45-krmax	$k_{soil-soot,max}$	Sect S4.3
46-ck0	ck_0	Sect S4.3
4-alpha_rain	α_{rain}	Sect S4.4
10-rhol_nir	$\rho_{l,nir}$	Sect S4.4

S4.1 Unsaturated water movement

Water flux between adjacent soil layers is calculated as (Dai et al., 2019):

$$q_{hm}(\Delta z, h_u, h_l) = -K_{hm} \cdot \left(\frac{h_l - h_u}{\Delta z} - 1\right), \tag{S1}$$

where q_{hm} is a function for calculating water flux within a homogeneous soil medium (mm s^{-1}), Δz is the thickness of the soil layer (mm), , h_u and h_l are the soil water potentials at the upper and lower boundaries of the soil layer, respectively (mm), and K_{hm} is the equivalent hydraulic conductivity (mm s^{-1}), which is the function of hydraulic conductivity K of soil layer and parameter r_0 associated with soil hydraulic model and parameters of soil hydraulic properties.

The soil hydraulic properties are then described using the van Genuchten–Mualem (VGM) model (Ippisch et al., 2006):

$$S_e = \begin{cases} \frac{1}{S_c} \cdot [1 + (\alpha\psi)^n]^{-m}, & \psi < \psi_s \\ 1, & \psi \geq \psi_s \end{cases}, \tag{S2}$$

$$S_e = \frac{\theta - \theta_r}{\theta_s - \theta_r}, \tag{S3}$$

$$S_c = [1 + (\alpha\psi_s)^n]^{-m}, \tag{S4}$$

$$m = 1 - \frac{1}{n}, \tag{S5}$$

$$K = K_s \cdot S_e^l \cdot \left[\frac{1 - \left(1 - (S_e S_c)^{1/m}\right)^m}{1 - \left(1 - S_c^{1/m}\right)^m}\right]^2, \tag{S6}$$

$$r_0 = \frac{1}{l(n-1) + 2n}, \tag{S7}$$

where S_e is the effective saturation (–), S_c is the saturation at the cut-off point (–), α is a shape parameter related to the inverse of the air-entry suction (mm^{-1}), n is a shape parameter representing the pore-size distribution (–), ψ is the unsaturated soil water potential (mm), ψ_s is the saturated matric potential (mm), θ is the volumetric water content (mm mm^{-3}), θ_r is the residual soil water content (mm mm^{-3}), θ_s is the saturated volumetric water content (mm mm^{-3}), K is the unsaturated hydraulic conductivity (mm s^{-1}), K_s is the saturated hydraulic conductivity (mm s^{-1}), and l is the pore-connectivity parameter (–).

S4.2 Subsurface runoff parameterization

Subsurface runoff is parameterized as (Niu et al., 2005):

$$r_{subsurface} = r_{sub,max} e^{-f_{drai} \times z_{wt}}, \tag{S8}$$

where $r_{subsurface}$ is the subsurface runoff (mm s^{-1}), $r_{sub,max}$ is the maximum subsurface runoff when the max grid cell mean water table depth is zero (with a model default value of 5.5 ×10^{-3} mm s^{-1}) (mm s^{-1}), f_{drai} is the decay factor (with a model default value of 2.5 m^{-1}) (m^{-1}), and z_{wt} is water table depth (m).

When soil ice is present, the impedance factor is applied (Niu and Yang, 2006):

$$f_{impd,ice} = 1 - \frac{e^{-\alpha_{ice} \times \left(1 - f_{ice,sum}\right)} - e^{-\alpha_{ice}}}{1 - e^{-\alpha_{ice}}}, \tag{S9}$$

$$r_{subsurface} = f_{impd,ice} \times r_{sub,max} e^{-f_{drai} \times z_{wt}}, \tag{S10}$$

where $f_{impd,ice}$ is the impedance factor accounting for the effect of ice on soil permeability (–), α_{ice} is an adjustable scale-dependent parameter with a prescribed value of 3 in the model (–), $f_{ice,sum}$ represents the total volumetric ice content within and below the soil layer where the water table is located (–).

S4.3 Plant hydraulics and transpiration processes

S4.3.1 Root transpiration

Root transpiration is the primary component of the source-sink term in the soil moisture governing equation. Root water uptake is driven by the water potential gradient between the soil and the roots (Van Den Honert, 1948; Kennedy et al., 2019; Amenu and Kumar, 2008; Zhu et al., 2017):

$$q_{root,i} = k_{soil-soot,i} \left(\psi_{soil,i} - \psi_{root,i}\right), \tag{S11}$$

where $q_{root,i}$ represents the radial water transport rate (s^{-1}), $k_{soil-soot,i}$ is the soil-and-root conductance (mm s^{-1}), $\psi_{soil,i}$ and $\psi_{root,i}$ denote the water potentials of the i-th soil node and the root node, respectively (mm).

The conductance is calculated as (Kennedy et al., 2019):

$$k_{soil-soot,i} = \frac{k_{root,i} \cdot k_{soil,i}}{k_{root,i} + k_{soil,i}}, \tag{S12}$$

$$k_{root,i} = \frac{k_{soil-soot,max}}{l_{root,lateral} + z_{soil,i}} \cdot RAI \cdot 2^{-\left(\frac{\psi_{soil,i}}{p50_{root}}\right)^{c_k}}, \tag{S13}$$

$$RAI = (LAI + SAI) \cdot r_i \cdot f_{root-leaf}, \tag{S14}$$

$$k_{soil,i} = \frac{\min\left(k_{sat,i}, k_{s,i}\right)}{1000 dx_{root,i}}, \tag{S15}$$

where $k_{root,i}$ and $k_{soil,i}$ are the root and soil hydraulic conductance, respectively (s^{-1}), $k_{soil-soot,max}$ is the root conductance per area and per length (mm s^{-1}), $l_{root,lateral}$ is the lateral root length (mm), $z_{soil,i}$ is the soil layer depth (mm), RAI is the

Root Area Index (–), $p50_{root}$ is the water potential at which 50% of root hydraulic conductivity is lost (mm), c_k is a shape factor fitting the vulnerability curve (–), SAI and LAI are the Stem and Leaf Area Indices (–), r_i is the root fraction (–), $f_{root-leaf}$ is a scaling ratio (–), $k_{sat,i}$ and $k_{s,i}$ represent the saturated and unsaturated hydraulic conductivity of the i-th layer (mm s^{-1}), $dx_{root,i}$ is the distance between roots (m).

For root fraction, the model utilizes the scheme ROOTFR_SCHEME = 1. For each land cover type n, the root fraction for each soil layer is defined as (Schenk and Jackson, 2002):

$$r_{i,n} = \begin{cases} \frac{1}{\left(1+\frac{100z_{soil,1}}{d_{50,n}}\right)^{\beta_n}}, i = 1 \\ \frac{1}{\left(1+\frac{100z_{soil,i}}{d_{50,n}}\right)^{\beta_n}} - \frac{1}{\left(1+\frac{100z_{soil,i-1}}{d_{50,n}}\right)^{\beta_n}}, i = 2, nl\_soil \\ 1 - \frac{1}{\left(1+\frac{100z_{soil,nl_{soil}-1}}{d_{50,n}}\right)^{\beta_n}}, i = nl\_soil \end{cases}, \tag{S16}$$

where z_{soil} is the interface depth (m), d_{50} is the depth containing 50% of the root system (m), β is a dimensionless shape factor (–).

S4.3.2 Plant Hydraulic

By default, CoLM sets DEF_USE_PLANTHYDRAULICS = .true., The vegetation hydraulic module calculates transpiration based on the Soil-Plant-Atmosphere Continuum (SPAC) concept, where water transport is driven by water potential gradients.

Assuming a steady-state water transport within the plant, the governing equations are as follows (Kennedy et al., 2019):

$$q_{sun\leftarrow stem} = k_{sun\leftarrow stem}(\psi_{sun} - \psi_{stem}), \tag{S17}$$

$$q_{sha\leftarrow stem} = k_{sha\leftarrow stem}(\psi_{sha} - \psi_{stem}), \tag{S18}$$

$$q_{stem\leftarrow root} = k_{stem\leftarrow root}(\psi_{stem} - \psi_{root,0}), \tag{S19}$$

where q denotes the water flux (mm s^{-1}), K represents the hydraulic conductance (s^{-1}), ψ is the water potential (mm), the subscripts sun, sha, $stem$, $root$, and root,0 represent sunlit leaves, shaded leaves, stem, root and root at surface, respectively.

Hydraulic conductance varies with changes in plant water potential. It is based on a sigmoidal vulnerability curve (Kennedy et al., 2019):

$$k_{i\leftarrow j} = k_{max} \cdot 2^{-\left(\frac{\psi_j}{p50}\right)^{c_k}}, \tag{S20}$$

where k_{max} is the maximum hydraulic conductance (s^{-1}), ψ_j is the water potential at node j (mm), $p50$ represents the water potential at which hydraulic conductance is reduced by 50% (mm), c_k is the shape parameter of the vulnerability curve (–).

Simultaneously, the above-ground water fluxes satisfy the following mass conservation equations (Kennedy et al., 2019):

$$E_{sun} = q_{sun\leftarrow stem}, \tag{S21}$$

$$E_{sha} = q_{sha\leftarrow stem}, \quad \text{(S22)}$$

$$q_{sha\leftarrow stem} + q_{sun\leftarrow stem} = q_{stem\leftarrow root}, \quad \text{(S23)}$$

$$q_{stem\leftarrow root} = q_{root,0}, \quad \text{(S24)}$$

where E_{sun} and E_{sha} represent the transpiration rates for sunlit and shaded leaves, respectively (mm s^{-1}). These rates are determined by the potential transpiration and a transpiration reduction function controlled by leaf water potential (Kennedy et al., 2019):

$$E_{sun} = E_{sun,max} \cdot 2^{-\left(\frac{\psi_{sun}}{p50}\right)^{c_k}}, \quad \text{(S25)}$$

$$E_{sha} = E_{sha,max} \cdot 2^{-\left(\frac{\psi_{sha}}{p50}\right)^{c_k}}, \quad \text{(S26)}$$

where $E_{sun,max}$ and $E_{sha,max}$ are the transpiration rates under non-water-stressed conditions (mm s^{-1}).

S4.4 Surface water input and energy balance

S4.4.1 Precipitation after interception

The model employs the CoLM2014 scheme by default (DEF_Interception_scheme = 1), where the net precipitation reaching the ground p_{rain} is defined as:

$$p_{rain} = \frac{x_{sc} + thru_{rain}}{\Delta t}, \quad \text{(S27)}$$

where p_{rain} is the net precipitation reaching the ground (mm s^{-1}), x_{sc} represents the excess water exceeding the maximum canopy storage capacity (mm), $thru_{rain}$ denotes the canopy throughfall from effective precipitation areas (mm), Δt is the time duration (s).

When calculating $thru_{rain}$ (with DEF_VEG_SNOW = .false.), it is assumed that only liquid water can be shed from the canopy (Lawrence et al., 2019):

$$thru_{rain} = (R_c + R_l)\Delta t\left(1 - \delta_p\right)\frac{a_p}{b}\left(1 - e^{-bx_s}\right) + c_p x_s + L_{dew} x_s - S_c x_s, \quad \text{(S28)}$$

$$\delta_p = 1 - \alpha_{rain} \times \left[1 - e^{-K_p \times LSAI}\right], \quad \text{(S29)}$$

where R_c and R_l are the convective and large-scale rainfall rates (mm s^{-1}), δ_p is the canopy throughfall coefficient (–), x_s represents the fraction of the saturated area (–), L_{dew} is the depth of water on the foliage (mm), S_c is the maximum canopy storage capacity (mm), α_{rain} is an empirical coefficient reflecting the water-holding capacity of leaves (–), K_p represents the extinction coefficient (–), and $LSAI$ represents the sum of LAI and SAI (–).

S4.4.2 Snowmelt and energy balance

The snowmelt rate s_m is driven by the energy surplus or deficit:

$$s_m = \max\left(0, \frac{H_i \Delta t / L_f}{\Delta t}\right), \quad \text{(S30)}$$

$$H_i = f\left(h_s, T, T_f, \alpha_{Grank}, F, c, \Delta t, \Delta z\right), \tag{S31}$$

where s_m is the snowmelt rate (mm s^{-1}), H_i is the energy surplus or deficit (W m^{-2}), L_f is the latent heat of fusion (J kg^{-1}), h_s is the net heat flux entering the surface (W m^{-2}), T is the temperature of the snow/soil (K), T_f is the freezing temperature (K), α_{Grank} is the Crank-Nicholson factor (–), F is the heat flux (W m^{-2}), c is the volumetric heat capacity (J m^{-3} K^{-1}), Δt is the times duration, and Δz is the soil layer thickness.

The net heat flux entering the ground surface, h_s, is expressed as follows:

$$h_s = S_g + L_g\left(T_g\right) - H_g\left(T_g\right) - \lambda E_g\left(T_g\right) + H_{prcg}\left(T_g\right), \tag{S32}$$

where S_g and L_g represent the net solar (shortwave) radiation and net longwave radiation absorbed by the ground surface (W m^{-2}), H_g is the sensible heat flux (W m^{-2}), λE_g is the latent heat flux (W m^{-2}), H_{prcg} is the sensible heat flux from precipitation (W m^{-2}), and T_g is the soil surface temperature (K).

The net solar radiation, S_g, is expressed as follows:

$$S_g = S_{vg} - S_{sun} - S_{sha}, \tag{S33}$$

where S_{vg} is the total solar shortwave radiation flux absorbed by the surface (including both ground and vegetation) (W m^{-2}), S_{sun} and S_{sha} represent the radiation absorption by sunlit and shaded leaves, respectively (W m^{-2}).

The total radiation flux absorbed by the vegetation-soil system is given by:

$$S_{vg} = S_{vis,dir}\left(1 - \alpha_{vis,dir}\right) + S_{vis,dif}\left(1 - \alpha_{vis,dif}\right) + S_{nir.dir}\left(1 - \alpha_{nir.dir}\right) + S_{nir.dif}\left(1 - \alpha_{nir.dif}\right), \tag{S34}$$

where S on the right-hand side represents the incoming solar shortwave radiation flux across different spectral bands (visible, vis; near-infrared, nir) (W m^{-2}) and radiation types (direct, dir; diffuse, dif) (W m^{-2}), and the term α is the albedo (–).

In the radiative transfer scheme, α_{veg} is a function of the leaf albedo ω (–), the Leaf Area Index LAI (–), the solar zenith angle μ (–), and the leaf angle distribution factor χ_L (–). Considering the canopy nir albedo, the albedo is defined as:

$$\alpha_{veg,nir} = f(w_{nir}, \mu, LAI, \chi_L), \tag{S35}$$

The albedo w_{nir} is defined as:

$$w_{nir} = \rho_{l,nir} + \tau_{l,nir}, \tag{S36}$$

where $\rho_{l,nir}$ is the leaf reflectance (–) and $\tau_{l,nir}$ is the leaf transmittance (–).

References

Amenu, G. G. and Kumar, P.: A model for hydraulic redistribution incorporating coupled soil-root moisture transport, Hydrol. Earth Syst. Sci., 12, 55-74, https://doi.org/10.5194/hess-12-55-2008, 2008.

Dai, Y., Zhang, S., Yuan, H., and Wei, N.: Modeling Variably Saturated Flow in Stratified Soils With Explicit Tracking of Wetting Front and Water Table Locations, Water Resour. Res., 55, 7939-7963, https://doi.org/10.1029/2019wr025368, 2019.

Ippisch, O., Vogel, H. J., and Bastian, P.: Validity limits for the van Genuchten–Mualem model and implications for parameter estimation and numerical simulation, Adv. Water Resour., 29, 1780-1789, https://doi.org/10.1016/j.advwatres.2005.12.011, 2006.

Kennedy, D., Swenson, S., Oleson, K. W., Lawrence, D. M., Fisher, R., Lola da Costa, A. C., and Gentine, P.: Implementing Plant Hydraulics in the Community Land Model, Version 5, J. Adv. Model. Earth Syst., 11, 485-513, https://doi.org/10.1029/2018MS001500, 2019.

Lawrence, D. M., Fisher, R. A., Koven, C. D., Oleson, K. W., Swenson, S. C., Bonan, G., Collier, N., Ghimire, B., van Kampenhout, L., Kennedy, D., Kluzek, E., Lawrence, P. J., Li, F., Li, H., Lombardozzi, D., Riley, W. J., Sacks, W. J., Shi, M., Vertenstein, M., Wieder, W. R., Xu, C., Ali, A. A., Badger, A. M., Bisht, G., van den Broeke, M., Brunke, M. A., Burns, S. P., Buzan, J., Clark, M., Craig, A., Dahlin, K., Drewniak, B., Fisher, J. B., Flanner, M., Fox, A. M., Gentine, P., Hoffman, F., Keppel-Aleks, G., Knox, R., Kumar, S., Lenaerts, J., Leung, L. R., Lipscomb, W. H., Lu, Y., Pandey, A., Pelletier, J. D., Perket, J., Randerson, J. T., Ricciuto, D. M., Sanderson, B. M., Slater, A., Subin, Z. M., Tang, J., Thomas, R. Q., Martin, M. V., and Zeng, X.: The Community Land Model Version 5: Description of New Features, Benchmarking, and Impact of Forcing Uncertainty, J. Adv. Model. Earth Syst., 11, 4245-4287, https://doi.org/10.1029/2018ms001583, 2019.

Niu, G.-Y. and Yang, Z.-L.: Effects of Frozen Soil on Snowmelt Runoff and Soil Water Storage at a Continental Scale, J. Hydrometeorol., 7, 937-952, https://doi.org/10.1175/JHM538.1, 2006.

Niu, G. Y., Yang, Z. L., Dickinson, R. E., and Gulden, L. E.: A simple TOPMODEL-based runoff parameterization (SIMTOP) for use in global climate models, J. Geophys. Res.-Atmos., 110, https://doi.org/10.1029/2005jd006111, 2005.

Schenk, H. J. and Jackson, R. B.: THE GLOBAL BIOGEOGRAPHY OF ROOTS, Ecological Monographs, 72, 311-328, https://doi.org/10.1890/0012-9615(2002)072[0311:TGBOR]2.0.CO;2, 2002.

van den Honert, T. H.: Water transport in plants as a catenary process, Discussions of the Faraday Society, 3, 146-153, https://doi.org/10.1039/DF9480300146, 1948.

Zhu, S., Chen, H., Zhang, X., Wei, N., Shangguan, W., Yuan, H., Zhang, S., Wang, L., Zhou, L., and Dai, Y.: Incorporating root hydraulic redistribution and compensatory water uptake in the Common Land Model: Effects on site level and global land modeling, J. Geophys. Res.-Atmos., 122, 7308-7322, https://doi.org/10.1002/2016JD025744, 2017.